

Cite this article as: Fu Junjian, Du Wenbo, Sun Jian, et al. In-vitro Degradation Behavior of Mg-4.0Zn-0.2Mn-0.2Ca Micro-tube Used for Biodegradable Vascular Stent[J]. Rare Metal Materials and Engineering, 2022, 51(05): 1572-1581.

ARTICLE

In-vitro Degradation Behavior of Mg-4.0Zn-0.2Mn-0.2Ca Micro-tube Used for Biodegradable Vascular Stent

Fu Junjian, Du Wenbo, Sun Jian, Adil Mansoor, Liu Ke, Du Xian, Li Shubo

Faculty of Materials and Manufacturing, Beijing University of Technology, Beijing 100124, China

Abstract: The in-vitro degradation behavior and corrosion mechanism of Mg-4.0Zn-0.2Mn-0.2Ca (wt%) micro-tube was investigated by the immersion tests and electrochemical tests. The results show that the corrosion resistance of the micro-tubes can be improved by the annealing treatment. The long-term immersion tests reveal that the corrosion process is relatively uniform, and the corrosion rate of the annealed micro-tube in Hank's solution is about 0.30 mm/a. During the initial stage of immersion, Mg(OH)₂ is formed on the surface of the annealed micro-tubes, forming a protective film to hinder the corrosion progress. Although the formed hydroxyapatite (HA) on Mg(OH)₂ film can further reduce the corrosion rate, the coarse secondary phases in Mg matrix can enhance the galvanic corrosion effect. The generated abundant hydrogen may destroy the HA film, thus promoting the corrosion process.

Key words: magnesium micro-tubes; corrosion; Hank's solution; corrosion mechanism; corrosion products

The coronary artery disease caused by the cardiovascular stenosis has become one of the major diseases affecting human health^[1,2]. With the development of percutaneous coronary intervention (PCI) technique, the implant of vascular stent is a common method to treat the coronary heart disease^[3-5]. The initial stent, such as bare metal stent (BMS) and drug eluting stent (DES), is made of stainless or cobalt chrome alloys. These stents usually remain in the blood vessel permanently, even when the tissue is recovered. Hence, it may cause a series of complications, such as in-stents restenosis (ISR) and thrombosis^[4]. The application of biodegradable stent (BDS) is a promising approach to overcome the shortcomings of permanent stents. During the first 3~6 months of implantation, BDS provides an effective mechanical force to support the occlusive target of arterial vessels. After the lesion of vessel tissue begins to reorganize, the stent gradually degrades and is absorbed. Theoretically, it requires 6~12 months for the complete repair of diseased vessel. Therefore, the stent needs to degrade at a uniform and slow rate to ensure the repair without sudden collapse. It is reported that the reasonable complete degradation duration of BDS after implantation is 12~24 months, depending on the

stent materials^[4,6,7].

BDSs are mainly made of biodegradable polymeric or metallic materials. The first generation of BDS is made of polymer due to its good formability. Nevertheless, the mechanical strength of polymer stent is usually weaker than that of the metal one, and cannot provide an effective radial supporting force during the vascular remodeling process, resulting in the acute wall recoil and late restenosis^[8]. Therefore, the biodegradable metallic vascular stent is proposed. Mg alloys show great potential because of their appropriate mechanical properties, excellent degradation performance, and good biocompatibility^[9-14]. In addition, Mg is the fourth abundant element in human body. The Mg²⁺ produced by Mg degradation participates in the human metabolism, and the excess Mg²⁺ is excreted through urinary system^[4,5]. Moreover, Mg element in human body has excellent performance of anti-platelet deposition and can reduce the thrombus tendency. Thus, Mg alloys are suitable for cardiovascular implant devices, especially for vascular stents^[15,16].

Despite the satisfactory performance of Mg alloys as vascular stents, their clinical application is still restricted due

Received date: September 17, 2021

Foundation item: National Key Research and Development Program of China (2016YFB0301101); Beijing Municipal Commission of Education Key Science and Technology Projects (KZ201810005005); National Natural Science Foundation of China (51801004); Beijing Natural Science Foundation, China (2192006)

Corresponding author: Du Wenbo, Ph. D., Professor, Faculty of Materials and Manufacturing, Beijing University of Technology, Beijing 100124, P. R. China, Tel: 0086-10-67392917, E-mail: duwb@bjut.edu.cn

Copyright © 2022, Northwest Institute for Nonferrous Metal Research. Published by Science Press. All rights reserved.

to the high corrosion rate (CR) and uncontrollable local corrosion. Currently, the corrosion behavior of Mg alloys has been widely investigated^[17-21], but the corrosion of processed Mg micro-tubes is rarely studied. Because the Mg vascular stent usually consists of micro-tubes prepared by laser engraving, the investigation on the corrosion behavior of Mg micro-tube can better reflect the actual status of vascular stent. Therefore, a new Mg-4.0Zn-0.2Mn-0.2Ca (wt%) alloy with good formability and excellent corrosion behavior was proposed^[22]. In this research, the Mg-4.0Zn-0.2Mn-0.2Ca alloy was processed to obtain the micro-tube with outer diameter of 3.6 mm and wall thickness of 0.4 mm through the hot-extrusion and drawing processes. Then the micro-tube was immersed in Hank's simulated body fluid (SBF) to study the in-vitro degradation behavior, including the corrosion microstructure, electrochemical behavior, and CR. The corrosion mechanism was also discussed.

1 Experiment

The cylindrical hollow billet of Mg-4.0Zn-0.2Mn-0.2Ca alloy with the length of 15 mm, outer diameter of 30 mm, and inner diameter of 6.5 mm was extruded at 380 °C with the extrusion ratio of 30:1 to obtain the tube blanks. Multi-pass drawing was conducted to manufacture the micro-tube. The drawing process included 7 passes without mandrel and 6 passes with fixed mandrel. After drawing, the micro-tube was fabricated with the outer diameter of 3.6 mm and wall thickness of 0.4 mm. Finally, the micro-tube was annealed at 300 °C for 30 min to eliminate the work hardening.

Microstructure observation was conducted on the optical microscope (OM, AXIO IMAGER A2M) and scanning electron microscope (SEM, HITACHI S3400N) coupled with energy dispersive spectroscope (EDS). The specimens for OM observation were ground with SiC paper, polished with diamond paste of 0.5 μm in size, and etched by 5vol% nitric acid/alcohol solution. The relative Volta potential difference between the secondary phase and Mg matrix was measured through the scanning Kelvin probe force microscope (SKPFM, Bruker Icon) in the tapping mode with a magnetic etched silicon probe (NSC18/Pt) at room temperature (~25 °C) under the relative humidity of ~50%. Before SKPFM experiment, the specimens were mechanically polished to 1 μm in thickness and cleaned using alcohol.

The electrochemical behavior was tested by an electrochemical workstation (Autolab, PGSTAT302N) with three-electrode system. The saturated calomel electrode (SCE), platinum mesh, and specimen were regarded as the reference electrode, counter electrode, and working electrode, respectively. The specimen (tube length of 10 mm) was cut into two pieces along the longitudinal direction, then cold-mounted into the epoxy resin. The exposed surface (longitudinal section) was ground with SiC paper and cleaned with alcohol. The Hank's solution was adopted as the electrolyte. The open circuit potential (OCP) of working electrode was monitored for 300~500 s before the potentiodynamic polarization tests. The potentiodynamic

polarization test was conducted at a constant scanning rate of 0.5 mV/s, and the range of test voltage of OCP was -300~300 mV. The electrochemical parameters, such as corrosion potential (E_{corr}) and corrosion current density (i_{corr}) were obtained by Tafel extrapolation method. Furthermore, the electrochemical impedance spectroscopy (EIS) measurements were conducted in the frequency range from 100 kHz to 100 mHz with a perturbation of 10 mV, and EIS data were fitted by ZView3.1 software. Each test was repeated three times to ensure the reproducibility of results.

The micro-tube was cut into pieces of 10 mm in length, ground by SiC paper, and cleaned by alcohol. The Hank's SBF solution was composed of 8.00 g/L NaCl, 0.40 g/L KCl, 0.14 g/L CaCl₂, 0.35 g/L NaHCO₃, 0.10 g/L MgCl₂·6H₂O, 0.06 g/L MgSO₄·7H₂O, 0.06 g/L KH₂PO₄, 0.06 g/L Na₂HPO₄·12H₂O, and 1.00 g/L C₆H₁₂O₆. The pH value was adjusted to 7.4 using NaOH or HCl before immersion, and the temperature was kept at 37.4 °C during the immersion. The ratio of the specimen surface to the volume of Hank's SBF solution was 1 cm²/150 mL according to ASTM G31-72. In order to ensure the accuracy, the Hank's SBF solution was changed every 6 d, and three parallel specimens were simultaneously conducted for each immersion experiment. The corrosion products were identified by X-ray diffraction (XRD). The specimen surface morphologies before and after removing corrosion products were observed by SEM. Then 3D profiles of the corroded surfaces were investigated by confocal laser scanning microscopy (CLSM). CR can be calculated by Eq.(1)^[23,24], as follows:

$$CR = \frac{K(W_0 - W_t)}{DTA} \quad (1)$$

where CR is the corrosion rate (mm/a); K is the constant of 8.76×10^4 ; W_0 and W_t are the mass before immersion and after removing the corrosion products (g), respectively; D is the density (g/cm³); A is the surface area exposed to the solution (cm²); T is the immersion time (h).

2 Results and Discussion

2.1 Microstructures and electrochemical properties of micro-tubes before and after annealing

Fig.1 shows the cross-section microstructures of Mg-4.0Zn-0.2Mn-0.2Ca micro-tubes before and after annealing. After the severe deformation of 13 passes, a large number of recrystallized grains and a few coarse irregular grains can be observed (Fig. 1a), indicating that the dynamic recrystallization occurs incompletely in micro-tubes before annealing. The non-uniform microstructure has a negative effect on corrosion of alloys. Fig.1b shows the uniform microstructure of the micro-tube after annealing. The grain size is about 4.0 μm. In addition, a few secondary phases precipitate in grains or on grain boundaries (Fig. 1c). EDS analysis in Fig. 1d indicates that the secondary phase at point A in Fig. 1c contains Mg, Zn, and Ca elements, and it is inferred as Ca₂Mg₆Zn₃. This result is consistent with the results in Ref.[23].

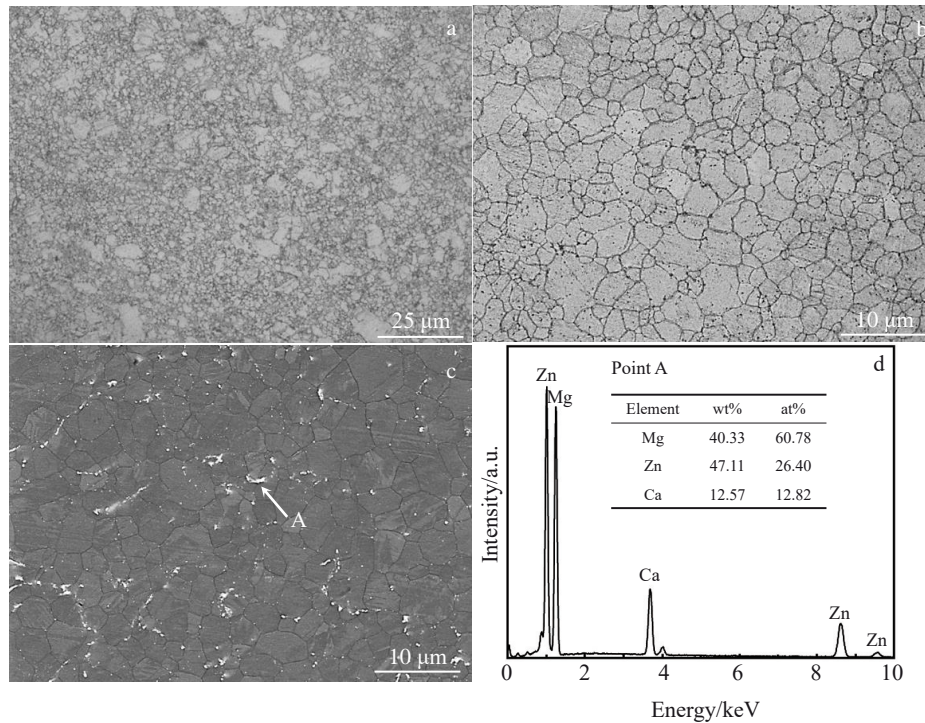


Fig.1 OM (a, b) and SEM (c) images of Mg-4.0Zn-0.2Mn-0.2Ca micro-tubes before (a) and after annealing (b, c); EDS analysis results of point A in Fig.1c (d)

Fig. 2a shows OCP of the Mg-4.0Zn-0.2Mn-0.2Ca micro-tubes before and after annealing in Hank's solution. The potential rises rapidly at the initial immersion stage, then slowly increases, and finally is stabilized at about -1.561 and -1.547 V vs. SCE for the micro-tubes before and after annealing, respectively. Moreover, the duration of achieving the stabilized potential of the micro-tube after annealing is longer than that before annealing. Generally, OCP reflects the corrosion resistance of materials: the higher the potential, the better the corrosion resistance^[25,26]. Thus, these results all infer that annealing is effective to enhance the corrosion resistance of micro-tubes.

Fig. 2b presents the potentiodynamic polarization curves of the specimens before and after annealing in Hank's solution. The detailed electrochemical parameters obtained by Tafel fitting are listed in Table 1. The corrosion current densities of the specimens before and after annealing are 2.96×10^{-6} and 1.95×10^{-6} A/cm², respectively. The lower corrosion current density of the annealed micro-tube indicates the enhanced corrosion resistance. Through the anodic polarization analysis (Fig. 2b), it is found that both the micro-tubes before and after annealing contain a passive zone, indicating that a protective film is formed on the micro-tube surface. When the protective film is destroyed, the corrosion continues, and the potential at this moment is regarded as the breakdown potential E_b ^[27]. The tested E_b of the micro-tubes before annealing (E_{b1}) and after annealing (E_{b2}) is -1.312 and -1.302 V vs. SCE, respectively. It demonstrates that the film formed on the annealed micro-tube surface is more stable and can provide better protection

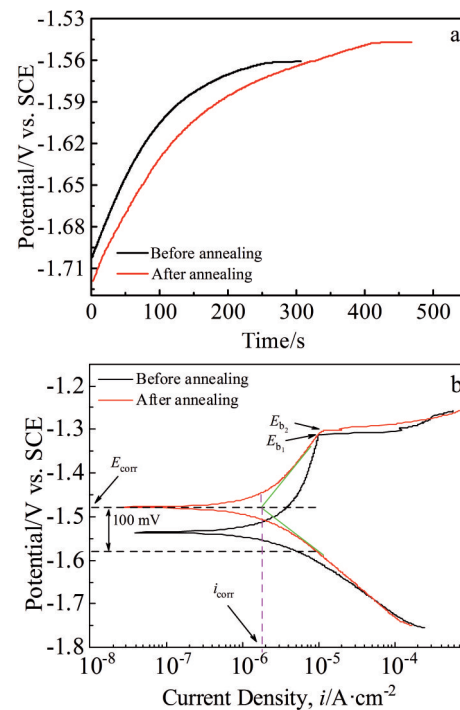


Fig.2 OCP (a) and potentiodynamic polarization curves (b) of Mg-4.0Zn-0.2Mn-0.2Ca micro-tubes before and after annealing

than the one on the micro-tube surface before annealing. In addition, the higher polarization resistance ($R_p=23.294$ kΩ) supports that the annealed micro-tube is more difficult to react

Table 1 Electrochemical parameters of Mg-4.0Zn-0.2Mn-0.2Ca micro-tubes before and after annealing

Parameter	Before annealing	After annealing
E_{corr}/V vs. SCE	-1.535	-1.478
E_b/V vs. SCE	-1.312	-1.302
$i_{\text{corr}}/\times 10^{-6} \text{ A}\cdot\text{cm}^{-2}$	2.96	1.95
$R_p/k\Omega$	15.561	23.294

with the Hank's solution, suggesting a better corrosion resistance.

EIS curves of the specimens after OCP measurement are shown in Fig. 3. The Nyquist plots of micro-tubes before and after annealing are composed of a capacitance loop at the high and middle frequencies, respectively; both of them have an inductive loop at the low frequency region. In addition, the equivalent circuit of the investigated specimens is identical, which indicates that they possess the same corrosion model. R_s represents the solution resistance, R_t represents the resistance of corrosion film, CPE_1 represents the constant phase element of corrosion film, CPE_2 represents the double layer capacitance. Meanwhile, n is the dispersion index of 0~1. CPE is identical to a pure resistance or a capacitor if n is equal to 0 or 1, respectively. R_{ct} is the charge transfer resistance, R_L is the inductance, and L is the inductance resistance, which indicates the breakdown of the corrosion film^[28]. χ^2 represents the accuracy of fitting. The smaller the value of χ^2 , the higher the fitting accuracy. The fitting results are summarized in Table 2,

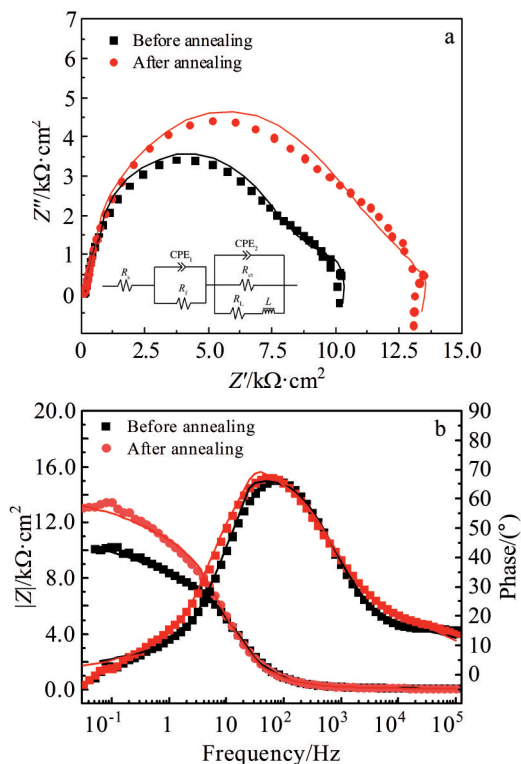


Fig. 3 Nyquist plots (a) and Bode plots (b) of Mg-4.0Zn-0.2Mn-0.2Ca micro-tubes before and after annealing

and the annealed micro-tube has larger values of R_{ct} , R_p , and R_L , indicating the better corrosion resistance. Furthermore, as shown in Fig. 3b, the larger phase peak width and impedance modulus ($|Z|$) can be found in the annealed micro-tube, which also demonstrates that the corrosion resistance of the annealed micro-tube is greater than that of the micro-tube without annealing.

2.2 In-vitro degradation of annealed micro-tubes

Fig. 4 shows the specimen surface morphologies of the annealed Mg-4.0Zn-0.2Mn-0.2Ca micro-tube after immersion in Hank's solution for 3, 7, and 14 d. All specimen surfaces are covered with a film of corrosion products, as shown in Fig. 4a~4c. With increasing the immersion time, the corrosion product is increased and becomes denser. Moreover, the cracks between the corrosion products become thick (as indicated by the red dotted lines in Fig. 4b). The denser film protects the specimens from the Hank's solution and hinders the corrosion process^[29]. Fig. 4d~4f show the surface morphologies after removing the corrosion products. Only a few corrosion pits can be found after immersion for 3 d, but the corroded area almost covers the entire surface after immersion for 7 d. The corrosion becomes more serious and the pits become deeper after immersion for 14 d.

Fig. 5a illustrates the corrosion rate of the annealed Mg-4.0Zn-0.2Mn-0.2Ca micro-tubes after immersion for different durations. The immersion can be divided into three stages: the first stage of 3~14 d, the second stage of 30~90 d, and the third stage of 120~180 d. The corrosion rate firstly decreases and then increases, which is 0.14~0.19 mm/a in the first stage, then decreased to 0.11~0.15 mm/a in the second stage, and finally increased to 0.27~0.30 mm/a in the third stage. Particularly, the corrosion rate remains the similar value of about 0.27 mm/a after immersion from 120 d to 150 d. Bian et al^[30] reported that the corrosion rate of ZM21 micro-tube after immersion in Hank's solution for 7 d is about 0.27 mm/a. Li et al^[31] reported the corrosion rate of 0.37 $\text{mg}\cdot\text{cm}^{-2}\cdot\text{h}^{-1}$ (about 18 mm/a) of Mg-Zn-Y-Nd micro-tube after immersion in SBF solution for 20 h. Compared with those research results, the micro-tube in this research shows excellent corrosion resistance. The corrosion rate is controlled by the surface corrosion product films. With increasing the immersion time, the corrosion product layer becomes heavy, so the corrosion rate is reduced in the second stage. Because this protective layer is unstable and can be destroyed by Cl^- ions, the corrosion rate becomes fast again in the third stage. Nevertheless, the corrosion rate of the annealed Mg-4.0Zn-0.2Mn-0.2Ca micro-tube can be controlled at a considerable value of about 0.30 mm/a during immersion within 180 d.

Fig. 5b shows the mass loss ratio of the annealed Mg-4.0Zn-0.2Mn-0.2Ca micro-tube as a function of immersion time. The micro-tube loses about 80% mass after immersion for 180 d. In addition, the micro-tube maintains the integrity of structure after immersion for 30 d, and the corrosion pits can be observed on the micro-tube surface since the specimen is immersed for 14 d. With increasing the immersion time, the size of corrosion pits is increased gradually, and the integrity

Table 2 Fitting results of EIS analyses

Treatment	$R_s/\Omega \cdot \text{cm}^2$	$R_f/\Omega \cdot \text{cm}^2$	$\text{CPE}_1/\times 10^{-6} \text{ F} \cdot \text{cm}^{-2}$	n_1	$\text{CPE}_2/\times 10^{-7} \text{ F} \cdot \text{cm}^{-2}$	n_2	$R_c/\Omega \cdot \text{cm}^2$	$R_L/\Omega \cdot \text{cm}^2$	$L/H \cdot \text{cm}^2$	$\chi^2/\times 10^{-3}$
Before annealing	53	6 616	4.43	0.96	5.66	0.50	9 878	206	38 970	2.84
After annealing	64	7 179	2.66	0.98	4.82	0.55	10 022	256	46 890	5.84

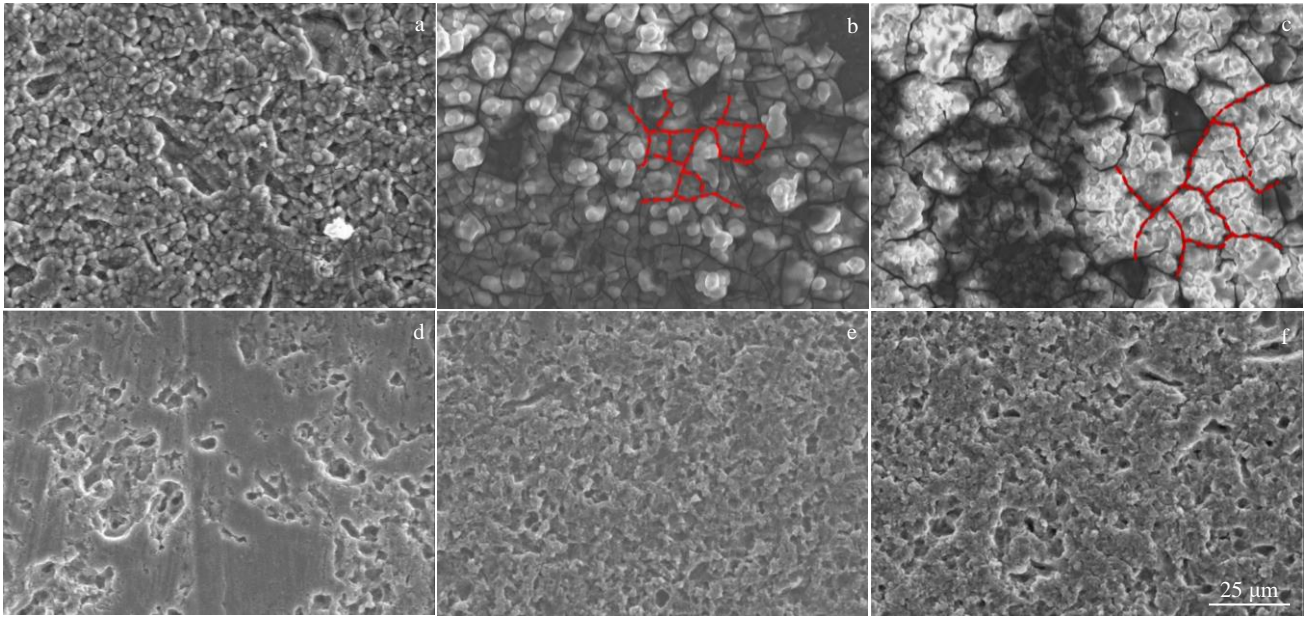


Fig.4 SEM images of surface morphologies of annealed Mg-4.0Zn-0.2Mn-0.2Ca micro-tubes before (a~c) and after (d~f) removing corrosion products after immersion for 3 d (a, d), 7 d (b, e), and 14 d (c, f)

of the micro-tube is destroyed. Generally, the vascular stent needs to provide sufficient support during the first six months after implantation. The Mg-4.0Zn-0.2Mn-0.2Ca micro-tube can meet the require, thereby presenting promising application potential as the vascular stent. Moreover, the in-vivo degradation rate of Mg alloys is much smaller than the in-vitro degradation rate^[32]. When the Mg-4.0Zn-0.2Mn-0.2Ca micro-tube is used as the vascular stent in human body, the real degradation rate should be much slower than that in this research.

2.3 Corrosion mechanism of annealed micro-tubes

2.3.1 Corrosion products

Fig. 6 shows SEM image and EDS analysis results of corrosion products of the annealed Mg-4.0Zn-0.2Mn-0.2Ca micro-tube after immersion for 14 d. It can be seen that the corrosion layer includes Mg, P, Ca, O, Cl, and Zn elements. EDS analysis of the gray-black product (point A) shows that the main elements are Mg and O, and their atomic ratio is close to 1:2. EDS result of the white corrosion product (point B) indicates that Mg content decreases, while the contents of

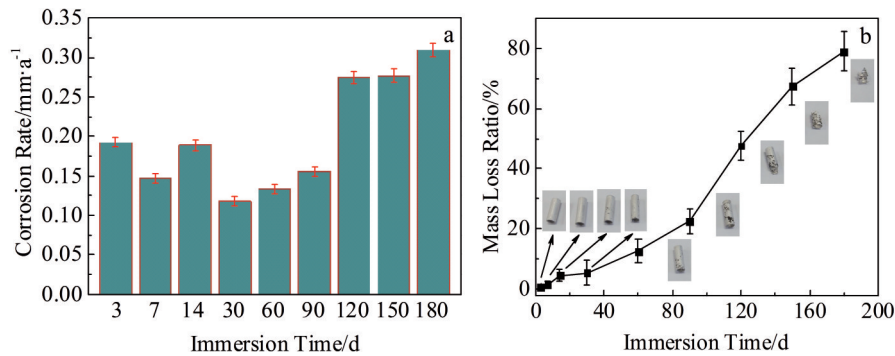


Fig.5 Corrosion rate (a) and mass loss ratio (b) of annealed Mg-4.0Zn-0.2Mn-0.2Ca micro-tubes after immersion for different durations

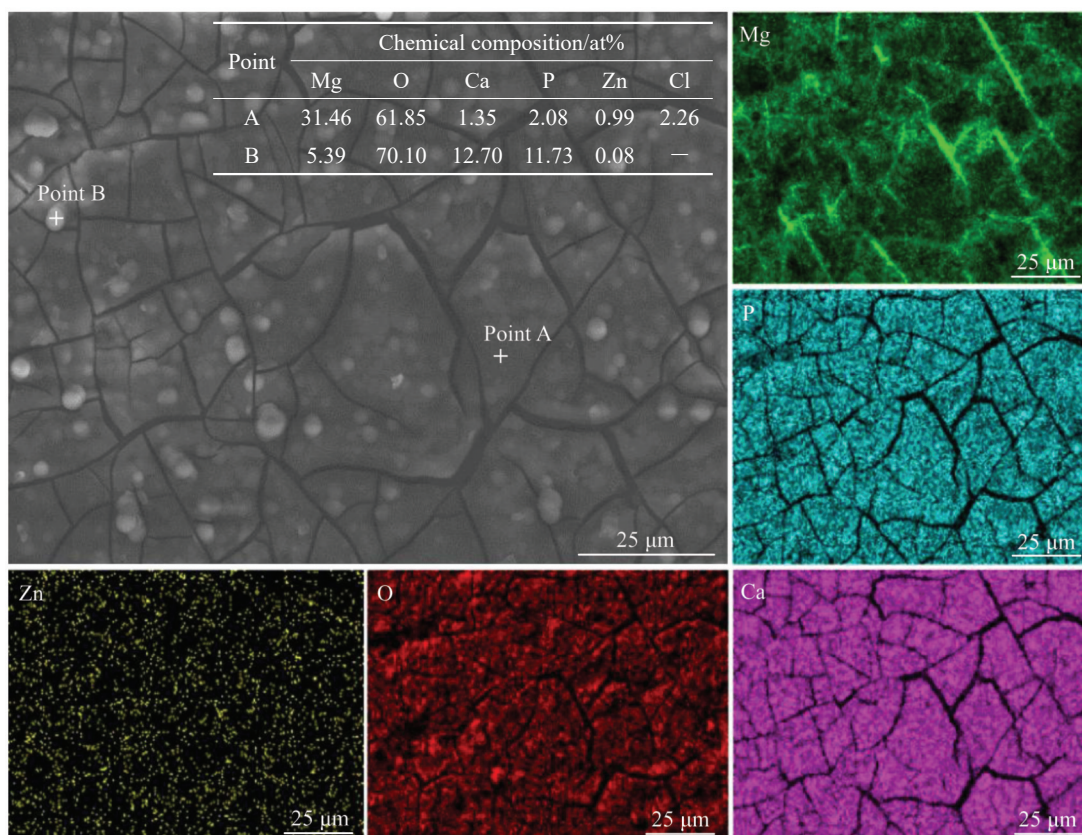


Fig.6 SEM image and corresponding EDS analysis results of corrosion products of annealed Mg-4.0Zn-0.2Mn-0.2Ca micro-tube after immersion for 14 d

P, O, and Ca elements obviously increase, compared with the results of point A. The composition of the white corrosion product is different from that of the gray-black one. Fig. 7 shows XRD pattern of the corrosion products of the annealed Mg-4.0Zn-0.2Mn-0.2Ca micro-tubes. The main components are $\text{Mg}(\text{OH})_2$, hydroxyapatite (HA), $(\text{Ca}, \text{Mg})_3(\text{PO}_4)_2$, and $\text{Ca}_2(\text{Mg}, \text{Zn})(\text{PO}_4)_2 \cdot \text{H}_2\text{O}$. Therefore, the gray-black and the white corrosion products are confirmed as $\text{Mg}(\text{OH})_2$ and HA, respectively. $\text{Mg}(\text{OH})_2$ is adhered to the surface to form the protective film at first. In the corrosion process, the phosphate

ions (PO_4^{3-}), carbonate ions (CO_3^{2-}), calcium ions (Ca^{2+}), and OH^- in the solution react with each other to form HA and then deposit on the $\text{Mg}(\text{OH})_2$ film^[33].

2.3.2 Corrosion mechanism

During the immersion of Mg-4.0Zn-0.2Mn-0.2Ca micro-tubes, the pH value of the Hank's solution changes and affects the corrosion process. Fig.8 shows the pH value variation as a function of immersion time. The pH value increases rapidly from 7.43 to 8.23 in the initial stage. After immersion for 8 h,

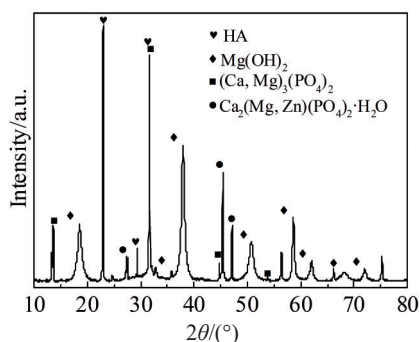


Fig.7 XRD pattern of corrosion products of annealed Mg-4.0Zn-0.2Mn-0.2Ca micro-tube

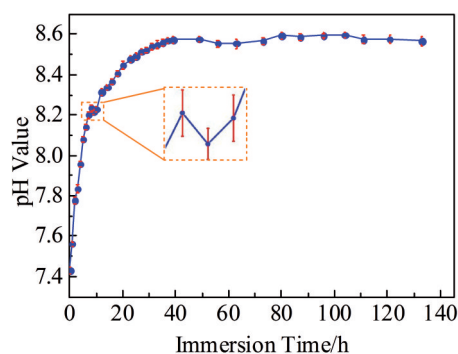


Fig.8 Relationship between pH value of Hank's solution and immersion time

a short platform appears. Then the pH value increases slowly and is finally stabilized at about 8.6.

Fig.9 shows the surface potential map around the secondary phases and the corresponding potential distribution along the marked line in Fig.9a. At SKPFM work function mode, the bright area suggests the area with higher potential. The secondary phases show a brighter color than the Mg matrix does and the Volta potential difference is about 272 mV, confirming that the $\text{Ca}_2\text{Mg}_6\text{Zn}_3$ phase is better than the Mg matrix and can act as micro-cathode during the corrosion process.

To further understand the corrosion behavior of Mg-4.0Zn-0.2Mn-0.2Ca micro-tube, CLSM was used to characterize the substrate surface without corrosion products. Fig. 10a~10c show 3D morphologies of the specimens after removing the corrosion products with immersion for different durations, and the corrosion depth curves are depicted in Fig.10d. It can be seen that the primary corrosion type of the micro-tube is the pitting corrosion.

Additionally, the number of corrosion pits is decreased correspondingly, but the pit size is increased with prolonging the immersion duration. After immersion for 3 d, it can be observed that the maximum corrosion depth is 15 μm . After immersion for 7 d, some corrosion pits connect with each other to form larger pits, and the maximum depth of the corrosion pit is increased to 100 μm . It can be seen from Fig.10c and 10d that a large through hole (the depth is about 400 μm , which is similar to the wall thickness of the micro-tube) is formed on the micro-tube surface after immersion for 30 d.

The $\text{Mg}(\text{OH})_2$ protective film is formed at the initial stage of corrosion, according to the following formulae^[34-36]:



Fig. 11 illustrates the schematic diagrams of the corrosion mechanism of Mg-4.0Zn-0.2Mn-0.2Ca micro-tubes in Hank's solution. At the beginning of corrosion (Stage I), the micro-tube surface is directly exposed to the solution. The corrosion process is accelerated at the secondary phase area, and the

larger corrosion pits are formed. During the immersion, Mg matrix is firstly corroded, because its standard electrode potential is lower than that of the secondary phase ($\text{Ca}_2\text{Mg}_6\text{Zn}_3$)^[15]. In the galvanic couple system, Mg anode loses electrons and turns into Mg^{2+} , and the hydrogen evolution reaction occurs at the cathode ($\text{Ca}_2\text{Mg}_6\text{Zn}_3$) to generate OH^- and H_2 (Fig.11a). The Mg^{2+} reacts with OH^- in the solution to form $\text{Mg}(\text{OH})_2$ when their concentrations reach to a certain level. Meanwhile, the abundant OH^- rapidly increases the pH value of solution in the initial stage of corrosion (Fig.8). In Stage II, with prolonging the immersion time, the $\text{Mg}(\text{OH})_2$ protective film is formed on the alloy surface (Fig.11b), hindering the contact between solution and substrate, and leading to the decrease in corrosion rate. The rate of hydrogen evolution slows down and the pH value is basically stable, so the short platform of pH value occurs in Fig. 8. Although the formed $\text{Mg}(\text{OH})_2$ protective film can hinder the corrosion, it is unstable and easily destroyed by the Cl^- ion in the Hank's solution. With the corrosion process further proceeding (Stage III), the aggressive anion (Cl^-) is absorbed onto the defects of the protective film, thereby forming the soluble chlorides with the cations. These soluble chlorides are active corrosion points, namely the pitting corrosion nucleus, which cause the pitting corrosion^[37]. After the pitting corrosion, the matrix under the protective film is exposed to the solution again, therefore generating new corrosion holes. Because the electrochemical potential of the secondary phases in the corrosion hole is lower than that of the matrix around the secondary phases, the galvanic cell is formed and the corrosion along the depth of corrosion hole is promoted, resulting in deeper and wider corrosion pits, as shown in Fig.11c.

Because the solubility product constant (K_{sp}) of HA is 1.6×10^{-58} , which is much lower than that of other products^[33], the Ca^{2+} , Mg^{2+} , PO_4^{3-} , and OH^- in the solution preferentially combine to form HA and then to deposit on the $\text{Mg}(\text{OH})_2$ film. HA is difficult to destroy by Cl^- ions, and can hinder the degradation of Mg matrix^[38]. However, the galvanic corrosion effect becomes stronger at the coarse secondary phase area, and the generated abundant hydrogen can destroy the HA film

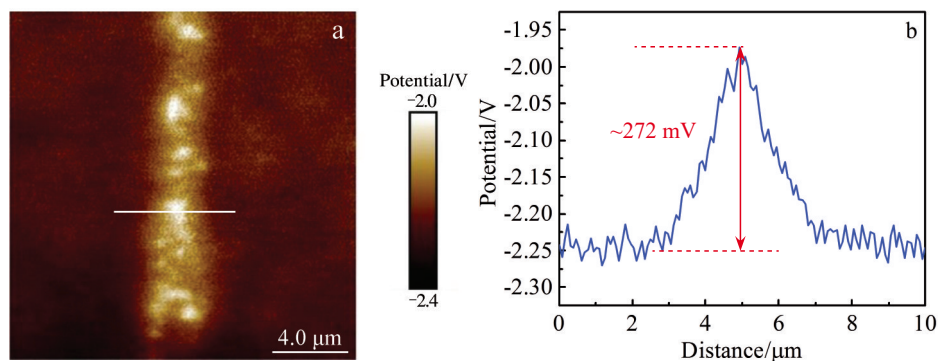


Fig.9 SKPFM results of annealed Mg-4.0Zn-0.2Mn-0.2Ca micro-tubes: (a) surface voltage potential map and (b) corresponding line scanning analysis of relative Volta potential of the secondary phases

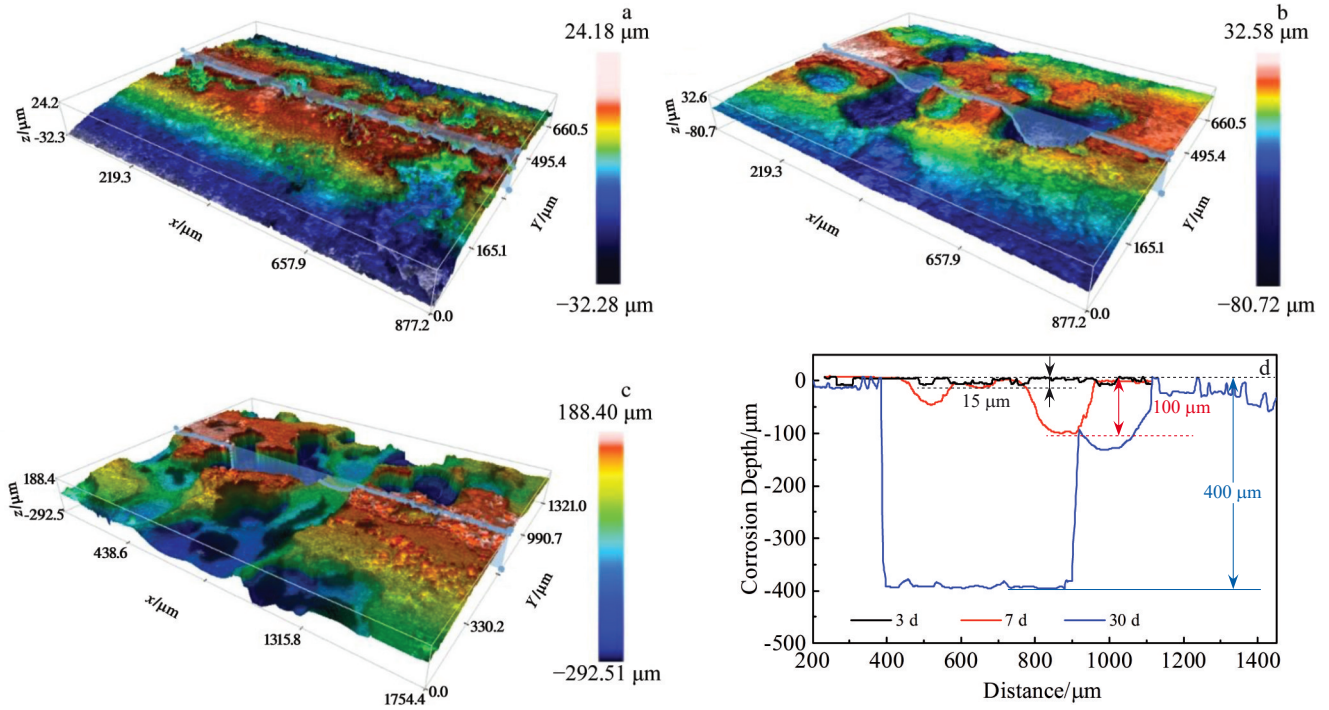


Fig.10 CLSM 3D profiles of Mg-4.0Zn-0.2Mn-0.2Ca micro-tubes after immersion in Hank's solution for 3 d (a), 7 d (b), and 30 d (c); corrosion depth profiles of Mg-4.0Zn-0.2Mn-0.2Ca micro-tubes along the sections in Fig.10a~10c (d)

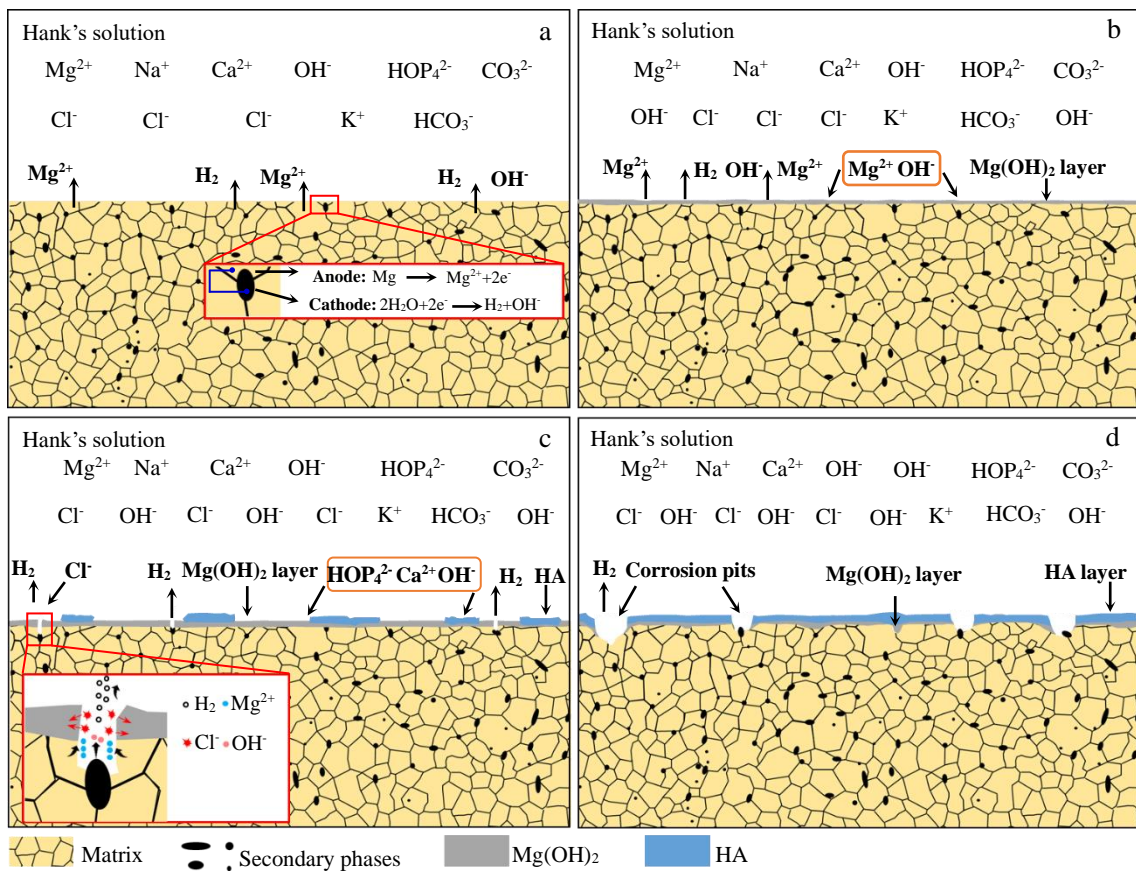


Fig.11 Schematic diagrams of corrosion evolution mechanism of Mg-4.0Zn-0.2Mn-0.2Ca micro-tube in Hank's solution: (a) Stage I, (b) Stage II, (c) Stage III, and (d) Stage IV

in Stage IV, leading to the initiation of corrosion process. Thus, the corrosion pits expand to the surrounding area or along the pit depth direction, as shown in Fig.11d.

3 Conclusions

1) Annealing is an effective approach to uniform the microstructure of Mg-4.0Zn-0.2Mn-0.2Ca micro-tube. The corrosion resistance of the micro-tube is improved after annealing.

2) The annealed micro-tube exhibits a slow corrosion rate of about 0.30 mm/a, indicating a good corrosion resistance performance.

3) During the immersion of the annealed micro-tubes, Mg(OH)₂ is firstly generated on the micro-tube surface, forming a protective film to hinder the corrosion. However, the Mg(OH)₂ film can be easily destroyed by H₂ and Cl⁻ in the solution, thereby leading to the pitting corrosion. Although the Ca²⁺, Mg²⁺, PO₄³⁻, and OH⁻ in the solution can form hydroxyapatite (HA) on Mg(OH)₂ film to reduce the corrosion rate, the coarse secondary phase increases the galvanic corrosion effect, and the generated abundant hydrogen can also destroy the HA film and promote the initiation of corrosion again.

References

- 1 Finegold J A, Asaria P, Francis D P. *International Journal of Cardiology*[J], 2013, 168(2): 934
- 2 McAloon C J, Boylan L M, Hamborg T et al. *International Journal of Cardiology*[J], 2016, 224: 256
- 3 Yang H T, Wang C, Liu C Q et al. *Biomaterials*[J], 2017, 145: 92
- 4 Hu T Z, Yang C, Lin S et al. *Materials Science and Engineering C*[J], 2018, 91: 163
- 5 Fu Junjian, Du Wenbo, Du Xian et al. *Rare Metal Materials and Engineering*[J], 2020, 49(10): 3576 (in Chinese)
- 6 Moravej M, Mantovani D. *International Journal of Molecular Sciences*[J], 2011, 12(7): 4250
- 7 Hermawan H, Dube D, Mantovani D. *Acta Biomaterialia*[J], 2010, 6(5): 1693
- 8 Pauck R G, Reddy B D. *Medical Engineering & Physics*[J], 2015, 37(1): 7
- 9 Witte F. *Acta Biomaterialia*[J], 2010, 6(5): 1680
- 10 Zheng Y F, Gu X N, Witte F. *Materials Science and Engineering R: Reports*[J], 2014, 77: 1
- 11 Wang J F, Zhou Y F, Yang Z Y. *Materials Science and Engineering C*[J], 2018, 90: 504
- 12 Homberger H, Virtanen S, Boccaccini A R. *Acta Biomaterialia* [J], 2012, 8(7): 2442
- 13 Zhang Z, Zhang J H, Wang J et al. *International Journal of Minerals, Metallurgy and Materials*[J], 2021, 28(1): 30
- 14 Yang M, Liu D B, Zhang R F et al. *Rare Metal Materials and Engineering*[J], 2018, 47(1): 93
- 15 Mao L, Zhou H, Chen L et al. *Journal of Alloys and Compounds* [J], 2017, 720: 245
- 16 Staiger M P, Pietak A M, Huadmai J et al. *Biomaterials*[J], 2006, 27(9): 1728
- 17 Zhang Y, Li J X, Li J Y. *Journal of the Mechanical Behavior of Biomedical Materials*[J], 2018, 80: 246
- 18 James M I, Wu G S, Zhao Y et al. *Corrosion Science*[J], 2015, 91: 160
- 19 Cihova M, Martinelli E, Schmutz P et al. *Acta Biomaterialia*[J], 2019, 100: 398
- 20 Cho D H, Lee B W, Park J Y et al. *Journal of Alloys and Compounds*[J], 2017, 695: 1166
- 21 Pan H, Pang K, Cui F Z et al. *Corrosion Science*[J], 2019, 157: 420
- 22 Du W B, Liu K, Ma K et al. *Journal of Magnesium and Alloys* [J], 2018, 6(1): 1
- 23 Cheng Y F, Du W B, Liu K et al. *Transactions of Nonferrous Metals Society of China*[J], 2020, 30(2): 363
- 24 Yao H, Xiong Y, Zha X Q et al. *Rare Metal Materials and Engineering*[J], 2021, 50(6): 1919
- 25 Lee Y L, Chu Y R, Li W C et al. *Corrosion Science*[J], 2013, 70: 74
- 26 Wang J F, Ma Y, Gao S F et al. *Materials & Design*[J], 2018, 153: 308
- 27 Chang J W, Fu P H, Guo X W et al. *Corrosion Science*[J], 2007, 49(6): 2612
- 28 Yin S Q, Duan W C, Liu W H et al. *Corrosion Science*[J], 2020, 166: 108 419
- 29 Zhou W R, Zheng Y F, Leeflang M A et al. *Acta Biomaterialia* [J], 2013, 9(10): 8488
- 30 Bian D, Jiang J J, Zhou W R et al. *Materials Letters*[J], 2018, 211: 261
- 31 Li W Q, Zhu S J, Sun Y F et al. *Journal of Alloys and Compounds*[J], 2020, 835: 155 369
- 32 Witte F, Fischer J, Nellesen J et al. *Biomaterials*[J], 2006, 27(7): 1013
- 33 Song Y W, Shan D Y, Chen R S et al. *Materials Science and Engineering C*[J], 2009, 29(3): 1039
- 34 Li Z J, Gu X N, Lou S Q et al. *Biomaterials*[J], 2008, 29(10): 1329
- 35 Wang X J, Chen Z N, Ren J et al. *Corrosion Science*[J], 2020, 164: 108 318
- 36 Qiao X Y, Yu K, Chen L J et al. *Rare Metal Materials and Engineering*[J], 2018, 47(3): 773
- 37 Yin S Q, Duan W C, Liu W H et al. *Corrosion Science*[J], 2020, 177: 108 962
- 38 Bakhsheshi-Rad H R, Abdul-Kadir M R, Idris M H et al. *Corrosion Science*[J], 2012, 64: 184

可降解血管支架用 Mg-4.0Zn-0.2Mn-0.2Ca 微细管的体外降解行为

付军健, 杜文博, 孙 健, Adil Mansoor, 刘 轲, 杜 宪, 李淑波

(北京工业大学 材料与制造学部, 北京 100124)

摘 要: 通过浸泡实验和电化学测试研究了 Mg-4.0Zn-0.2Mn-0.2Ca (质量分数) 微细管的体外降解行为与腐蚀机理。结果表明, 退火处理可以提高微细管的耐腐蚀性。长期浸泡实验表明腐蚀过程相对均匀, 退火微细管在 Hank's 溶液中的腐蚀速率约为 0.30 mm/a。在浸泡初期, 退火管材表面生成 $Mg(OH)_2$, 形成保护膜, 阻碍腐蚀进行。虽然 $Mg(OH)_2$ 膜上形成的羟基磷灰石 (HA) 可以进一步降低腐蚀速率, 但是镁基体中粗大的第二相会增强电偶腐蚀效应, 并且生成的大量氢气, 从而破坏 HA 膜, 使腐蚀继续进行。

关键词: 镁微细管; 腐蚀; Hank's 溶液; 腐蚀机理; 腐蚀产物

作者简介: 付军健, 男, 1991 年生, 博士, 北京工业大学材料与制造学部, 北京 100124, E-mail: fujunjian@emails.bjut.edu.cn